

NRC Publications Archive Archives des publications du CNRC

Modeling of microstructural evolution in hard turning of AISI-52100

Thai, Lam-Ngoc; Shi, Bin; Attia, Helmi; Plourde, Benoit; McMahon, Christian;
Grenon, Jean-David

This publication could be one of several versions: author's original, accepted manuscript or the publisher's version. /
La version de cette publication peut être l'une des suivantes : la version prépublication de l'auteur, la version
acceptée du manuscrit ou la version de l'éditeur.

For the publisher's version, please access the DOI link below. / Pour consulter la version de l'éditeur, utilisez le lien
DOI ci-dessous.

Publisher's version / Version de l'éditeur:

<https://doi.org/10.1016/j.procir.2023.03.019>

Procedia CIRP, 117, C, pp. 104-109, 2023-05-02

NRC Publications Archive Record / Notice des Archives des publications du CNRC :

<https://nrc-publications.canada.ca/eng/view/object/?id=e42f5705-9ea8-42d2-ac93-6eb7cbb9d1d4>

<https://publications-cnrc.canada.ca/fra/voir/objet/?id=e42f5705-9ea8-42d2-ac93-6eb7cbb9d1d4>

Access and use of this website and the material on it are subject to the Terms and Conditions set forth at

<https://nrc-publications.canada.ca/eng/copyright>

READ THESE TERMS AND CONDITIONS CAREFULLY BEFORE USING THIS WEBSITE.

L'accès à ce site Web et l'utilisation de son contenu sont assujettis aux conditions présentées dans le site

<https://publications-cnrc.canada.ca/fra/droits>

LISEZ CES CONDITIONS ATTENTIVEMENT AVANT D'UTILISER CE SITE WEB.

Questions? Contact the NRC Publications Archive team at

PublicationsArchive-ArchivesPublications@nrc-cnrc.gc.ca. If you wish to email the authors directly, please see the
first page of the publication for their contact information.

Vous avez des questions? Nous pouvons vous aider. Pour communiquer directement avec un auteur, consultez la
première page de la revue dans laquelle son article a été publié afin de trouver ses coordonnées. Si vous n'arrivez
pas à les repérer, communiquez avec nous à PublicationsArchive-ArchivesPublications@nrc-cnrc.gc.ca.

19th CIRP Conference on Modeling of Machining Operations

Modeling of Microstructural Evolution in Hard Turning of AISI-52100

Lam-Ngoc Thai^a, Bin Shi^b, Helmi Attia^{a,b,*}, Benoit Plourde^c, Christian McMahon^c, Jean-David Grenon^c

^aMcGill University, Department of Mechanical Engineering, 817 Sherbrooke St W, Montreal QC H3A 0C3, Canada

^bAerospace Manufacturing, National Research Council of Canada (NRC), 5145 Decelles Avenue, Montreal QC H3T 2B2, Canada

^cSainte-Julie, QC J3E 1Z8, Canada

* Helmi Attia, Tel.: 1-514-2396852; E-mail address: helmi.attia@mcgill.ca

Abstract

White layers formed during machining of AISI-52100 decrease the fatigue life of dynamically loaded components. It is critical to predict the temperature and microstructure evolution of machined surfaces. This research examined 3D simulation of hard turning using a round insert. Voce-Johnson Cook constitutive law and hardness-based microstructural evolution model were incorporated. To reduce the excessive computational time, the 3D simulation was simplified to a 2D simulation. The predicted cutting forces, temperature, and microstructure changes were validated against experimental data. The results showed the accuracy of the process simulation for process optimization in order to avoid white layer formation.

© 2023 The Authors. Published by Elsevier B.V.

This is an open access article under the CC BY-NC-ND license (<https://creativecommons.org/licenses/by-nc-nd/4.0>)

Peer review under the responsibility of the scientific committee of the 19th CIRP Conference on Modeling of Machining Operations

Keywords: Modeling; hard turning; white layer

1. Introduction

White layers formed in machining are characterized by their relatively high hardness and low ductility. They are responsible for increased formation and propagation of cracks, and consequently, a decrease in the fatigue life of dynamically loaded components. The white layer is formed dominantly due to thermally-induced phase transformation that occurs at high temperature during machining [1]. Therefore, it is critical to simulate the machining process and accurately predict the temperature rise at the tool–workpiece interface and the microstructure evolution of machined surfaces.

Most research has made use of the plane strain condition of the turning process to simulate it as a 2D problem. However, the plane strain condition cannot always be assumed, especially when the geometries of the tool and the workpiece are complex and can only be correctly simulated in 3D. However, 3D simulation requiring large number of elements is usually computationally expensive. Some researchers employed the Arbitrary Lagrangian Eulerian (ALE) method to simulate 3D

hard turning. This method requires a predefined initial chip geometry. Arrazola and Özel [2] first run a few steps with manual remeshing and interpolation. When the steady state with the final contact length was reached, the ALE method with Eulerian boundaries was then applied to reach the final state. This method was also used by Attanasio et al. [3] and was compared with the conventional incremental Lagrangian (IL) method. The ALE method was much faster but produced less accurate results compared to the IL method. Other researchers have applied the explicit finite element method (FEM) to reduce the computational time [4, 5]. Iynen et al. [5] coupled the explicit FEM with chip formulation using an element deletion technique and mesh quality enhancement using ALE. Advanced software packages with adaptive remeshing capability, such as AdvantEdge or Deform, were also employed to facilitate the 3D simulations [6-9].

To deal with practical hard turning operations, this research has focused on 3D modelling and simulation of turning operations to consider the complex geometric features of the workpiece and the use of round cutting tool inserts.

The FE process model incorporates Voce-Johnson Cook constitutive law and hardness-based microstructural evolution. The predicted cutting forces, temperature profile, and microstructure evolution were validated against the results obtained from hard turning experiments of AISI-52100. The effect of the cutting speed and feed rate on the microhardness distribution in the subsurface layer of the machined surface, and the white layer formation were investigated. To significantly reduce the computational time, the 3D model was reduced to a 2D model that accounts for the variable uncut chip thickness. The results showed the accuracy of the process simulation and the validity of the proposed approach to improve the computational efficiency using a 2D model. Process optimization using the proposed model to avoid white layer formation is demonstrated.

2. Experimental Work

The turning experiments were conducted using AISI 52100 workpiece and a round ceramic insert with chamfered and rounded edge (CeramTec RNGN 120400 S-S WXM255) as shown in Fig. 1. A negative rake angle of -8.5° was provided by the tool holder. Flood coolant was applied at pressure of 0.38 MPa and flow rate of 6.4 L/min. Cutting forces were measured using Kistler dynamometer model 9121 attached to the tool holder.

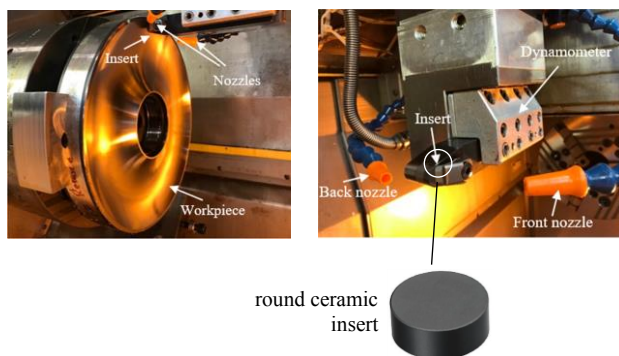


Fig. 1. Experiment set-up.

An initial cutting pass was performed to ensure a uniform depth of cut (0.3 mm), which was used for all the tests. The cutting speeds and feeds applied in the experiments are shown in Table 1.

Table 1. Cutting conditions.

Test	Feed (mm/rev)	Cutting speed (m/min)
1	0.17	200
2	0.17	150
3	0.17	100
4	0.23	150
5	0.3	150

After the turning experiments, the microstructure of the machined surface was examined to determine its properties. The workpiece was sectioned into small samples by wire electrical discharge machining as shown in Fig. 2a. These

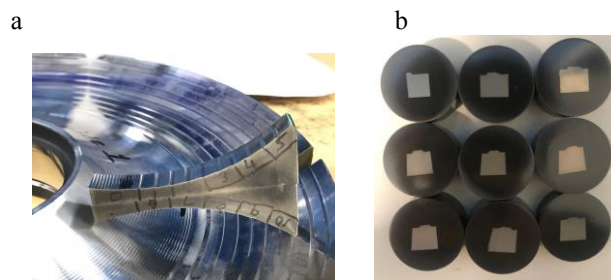


Fig. 2. Samples (a) before mounting; (b) after mounting.

samples were mounted into phenolic resins as seen in Fig. 2b. The mounted samples were then ground, polished, and etched with Nital 2% to reveal the microstructural grains, which could be observed through microscope (Olympus GX 71) at the magnification factor of 100x. The white and dark layers were measured at various locations along the machined surfaces.

Fig. 3 shows an example of white and black layers using a sample from Test 2.

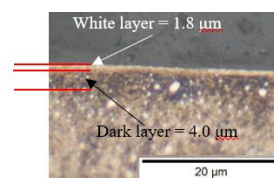


Fig. 3. Microscopic photo of a sample from Test 2.

3. Finite element modeling

3.1. 3D simulation

The turning process was modelled in 3D using DEFORM-3D V13.0 software [10]. The geometries of the tool and workpiece were imported into the software.

The workpiece was modelled as a rigid-plastic object. The closer to the contact with the tool, the finer was the mesh in order to capture the large temperature gradient near the contact zone. The element size ranged from 0.01 to 1 mm. The tool was modelled as a rigid object with the minimum mesh size of 0.02 mm around the contact region with the workpiece. The model is shown in Fig. 4.

The workpiece was constrained in all three directions at the bottom surface and the tool was set to move along the cutting direction at the given cutting speed. All surfaces of the

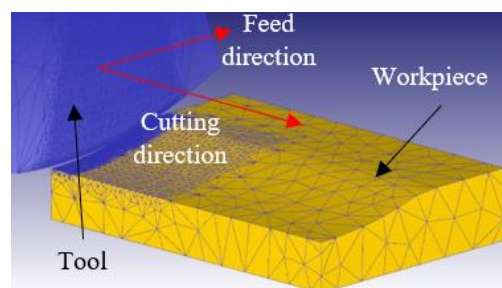


Fig. 4. 3D Finite Element model.

workpiece and tool were set to exchange heat with the surrounding.

The thermo-mechanical properties of workpiece and tool materials are shown in Table 2.

Table 2. Properties of workpiece and tool materials.

	AISI 52100	WXM 255
Thermal conductivity (W/mK)	24.5	30
Specific heat (J/kgK)	637	774
Density (kg/m ³)	7850	3800
Emissivity	0.7	0.03

The plastic flow stress of AISI 52100 was expressed by the modified Johnson Cook model coupled with Voce hardening law [11]. Orthogonal cutting tests were carried out to identify the material constants using the methodology developed by the authors [12, 13]. The identified material model is expressed as:

$$\sigma = (1195 - 548e^{-2.01\varepsilon}) \left(1 + 0.05 \ln \frac{\dot{\varepsilon}}{\dot{\varepsilon}_0} \right) \left[1 - \left(\frac{T - T_0}{T_m - T_0} \right)^{0.736} \right] \quad (1)$$

where σ is the flow stress, ε and $\dot{\varepsilon}$ are the effective strain and strain rate, respectively, $T_0 = 20^\circ\text{C}$ (room temperature), $T_m = 1424^\circ\text{C}$ is the material melting point, and $\dot{\varepsilon}_0 = 10^{-3} \text{ s}^{-1}$ is the reference strain rate.

The friction at the tool-chip interface was modelled as constant shear friction. To determine the friction coefficient μ , the simulation of a single combination of cutting conditions was repeated with a friction coefficient ranging from 0.65 to 0.85 and the resulting simulated force was compared with the experimental force measurement. The friction coefficient of coefficient $\mu = 0.85$ was selected for the remaining simulations. As will be shown in in section 4.1, the maximum prediction error for all the five cases is $< 15\%$. The heat transfer coefficient between the tool and workpiece was $100 \text{ kW/m}^2 \text{ }^\circ\text{C}$ as most cutting speeds can be modelled accurately using this value [14].

3.2. 2D simulation

Despite its accurate simulation of the turning process, the 3D finite model is computational expensive and each run takes around 3-4 days using a computer with Intel i7-5820L CPU@3.3GHz, 6 cores and 48GB RAM. Therefore, the 3D model was simplified into 2D to reduce the simulation time. This reduction in computational cost allows the finer mesh size in 2D simulation, enabling the modelling of microstructure transformation.

Due to the geometry of the cutting insert, the uncut chip thickness varies along the cutting edge. At any location along the curved machined surface, the uncut chip thickness could be computed and applied into a 2D model as shown in Fig. 5. The uncut chip thickness can be expressed as a function of the

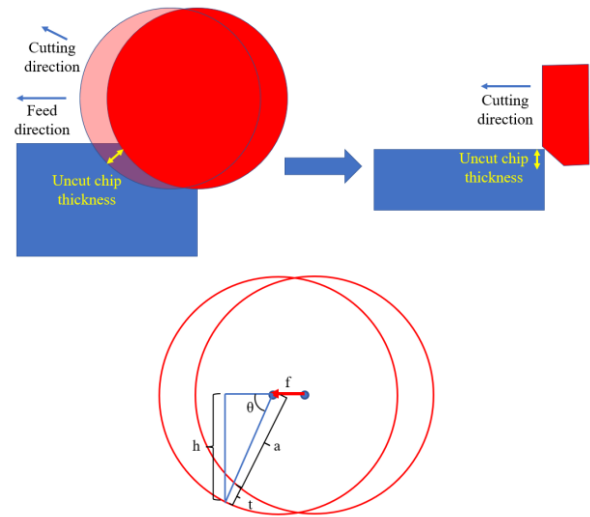


Fig. 5. Simplifying the 3D model into a 2D model.

cutting feed and vertical distance from the centre of the insert to the contact with the workpiece as follows:

$$t = R - \frac{R}{\sin(\pi - \theta)} \sin \left[\theta - \sin^{-1} \left(\frac{R}{f} \sin(\pi - \theta) \right) \right] \quad (2)$$

where R is the tool's radius, f is cutting feed and h is the vertical distance from the centre of the insert to the contact with the workpiece. The angle θ is determined as follows:

$$\theta = \sin^{-1} \left(\frac{h}{R} \right) \quad (3)$$

Similar to the 3D model, the region of the workpiece near the tool also had much finer mesh than other regions. The mesh in 2D model was much more refined than in 3D model to facilitate the simulation of microstructural evolution. Such fine mesh is not feasible in 3D models as it would be too time-consuming. The mesh size ranged from 0.0005 to 4 mm for the 2D model. The bottom of the workpiece was constrained in both directions and the tool was set to move at the cutting speed. The materials and inter-material's properties were the same as the 3D model. The 2D model is shown in Fig. 6.

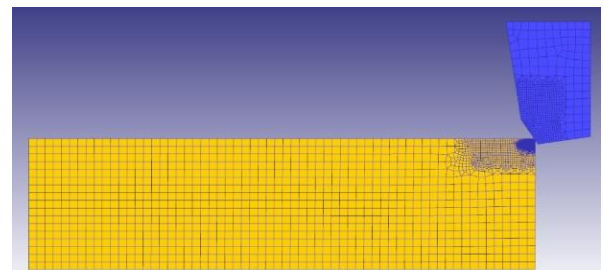


Fig. 6. 2D Finite Element model.

In order to simulate the formation of white and black layers, a hardness-based microstructural transformation model [15] was applied for every element of the workpiece.

The white layer is formed when the temperature exceeds the austenite-start temperature. The hardness of the white layer is updated as:

$$\Delta HRC = 10.8 \left[\frac{67 - HRC_i}{1030 - T_{AUS}} \right] (T - T_{AUS}) \quad (4)$$

where HRC_i is the initial hardness of AISI 52100 and T is the current element temperature. The temperature T refers to the predicted temperature at each nodal point in the FE model. The change in hardness at each increment is determined by the current temperature of the element at that time step.

The dark layer is formed when the temperature is above the tempering-start temperature, $T_{DLSTART}$ and below the austenite-start temperature, T_{AUS} . The hardness of the white layer is updated as:

$$\Delta HRC = 0.58 \left[\frac{HRC_i - 43}{T_{AUS} - T_{DLSTART}} \right] (T_{DLSTART} - T) \quad (5)$$

The tempering-start and austenite-start temperatures are 500°C and 640°C, respectively.

4. Results and Discussions

4.1. Validation of 3D model

The cutting force from the simulation was validated against the experimental result. The results from Tests 1 and 5 are shown in Fig. 7. The cutting forces from the simulation agree with the experiment within 15% for all the five cases listed in Table 1. This error is quite acceptable for FE simulations, considering the measurement uncertainty. Since the minimum mesh size of the workpiece in the 3D model is still much larger than the thicknesses of the white and dark layers, it is not possible to simulate the microstructural evolution and therefore, this was not validated for the 3D model.

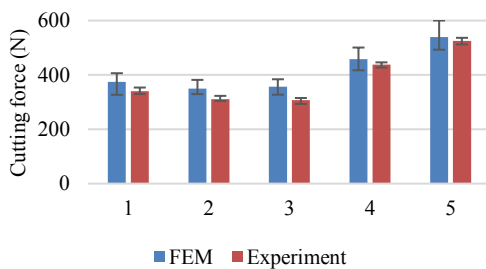


Fig. 7. Comparison of simulated and experimented cutting forces.

4.2. Validation of 2D model

To ensure that the simplified 2D model can accurately predict the 3D turning process, the temperature prediction of the 2D model was validated against the 3D model and the results from Test 1.

First, the temperature profiles below the machined surface of Test 1 were compared between the 2D and 3D models, as shown in Fig. 8. The maximum temperatures at the machined surface were 649°C and 643°C for the 2D and 3D simulations, respectively. Similar temperature profiles under the machined surface could also be observed between the 2D and 3D simulations. The temperature histories at a fixed location of machined surfaces were also compared between the 2D and 3D

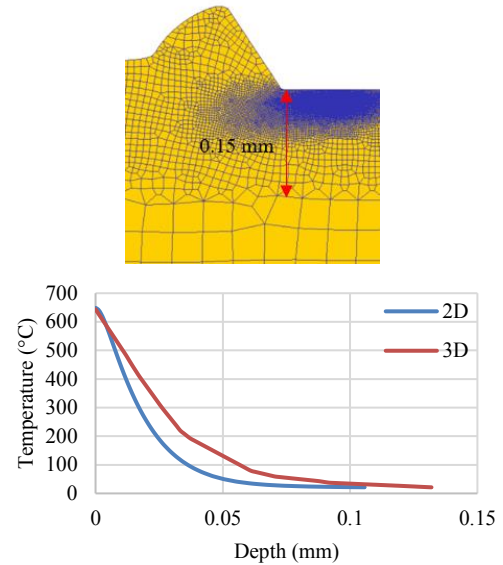


Fig. 8. Temperature variation below the machined surface.

models as seen in Fig. 9. Similar temperature history can be observed between the two models.

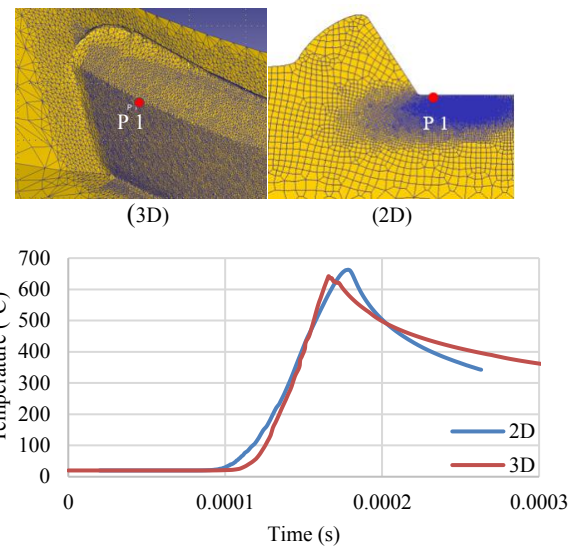


Fig. 9. Time variation of temperature at point P on the machined surface.

Since the temperature profile obtained from the 2D model agrees well with the 3D model, this 2D model can then be used to simulate the remaining tests and predict the microstructural transformation.

4.3. Microstructural transformation

The hardness-based microstructural transformation model was incorporated into the 2D model. This allowed the hardness of every element to be updated at every time step and the microstructure to be predicted based on the hardness value. A region with hardness value higher than the hardness of the base material is the white layer and the one with the hardness value lower than the hardness of the base material is the dark layer.

The initial hardness of AISI 52100 used in this experiment is 63 HRC.

The variation of hardness below machined surface for Tests 1-3 is shown in Fig. 10. For Tests 1 and 2, the hardness at the machined surface is higher than the hardness of the base material, indicating the presence of the white layer. The absence of this high hardness values in Test 3 means that there is no white layer present.

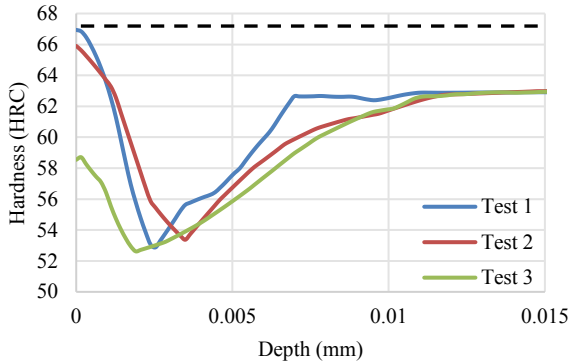


Fig. 10. Hardness profile below machined surface.

For all three tests, the hardness decreases with increasing depth below the machined surface, indicating the formation of a dark layer. After reaching the minimum value, the hardness value increases again, approaching the hardness of the base material.

The white layer thickness obtained from the 2D model was validated against the experimental results as shown in Fig. 11. The simulated results agree with the experimental results within 12%, with the exception of Test 1 with the error of 37.5%. This is because the mesh size of 0.5 μm cannot accurately capture the white layer thickness of 0.8 μm. Usually, the mesh size should be at most half of the expected layer to

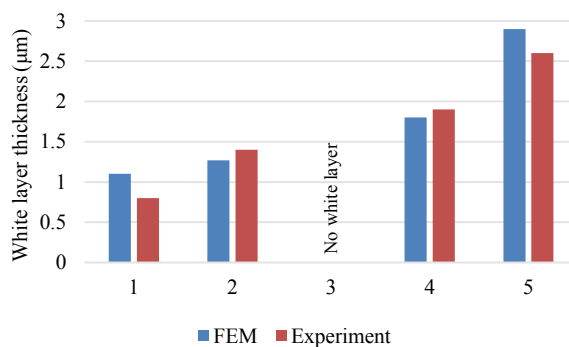


Fig. 11. White layer thickness obtained from simulations and experiments

produce accurate results. Although it is possible to further reduce the mesh size of the workpiece, this will significantly increase running time.

Fig. 12 shows the comparison between the dark layer thickness from the simulation and experiment. There was a large error of 60% for most tests between the two results. This can be attributed to two main reasons. The first reason is the inaccuracy of the 2D model at increasing depth below the

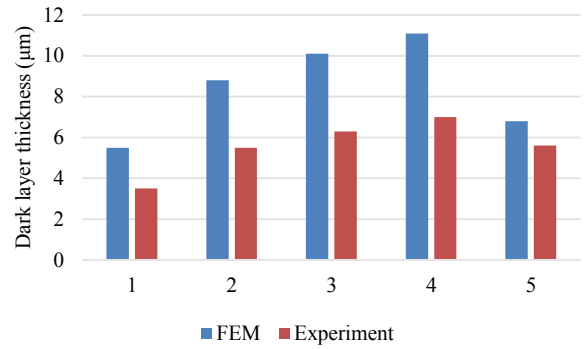


Fig. 12. Dark layer thickness obtained from simulations and experiments.

machined surface. This can be observed in Fig. 8. Up to 5 μm below the machined surface, the temperature profiles of the 2D and 3D models are almost identical. Beyond 5 μm, the temperature obtained from the 2D model starts to deviate from that of the 3D model. This explains why the 2D model can accurately predict the white layer, which occurs at a shallower level but not the dark layer. The second reason is the difficulty in distinguishing the dark layer observed from the experiment. At high cutting speeds, the temperature below the machined surface decreases quickly, coupled with high strain rate. This limits the dynamic recrystallization process, which forms the dark layer [16].

The effects of the cutting speed and the feed on the white layer thickness were also investigated. The effect of feed on the white layer thickness is shown in Fig. 13. At a constant cutting speed of 150 m/min, the white layer thickness increases with increasing feed due to the increased cutting temperature.

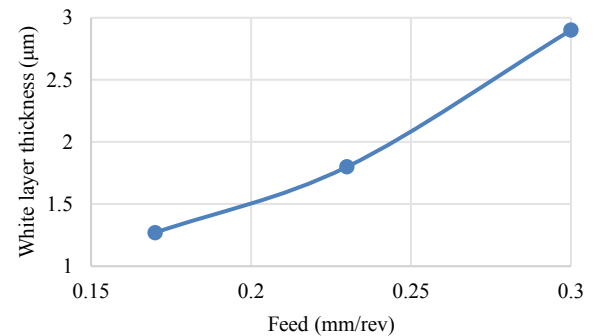


Fig. 13. White layer thickness at various feeds and constant cutting speed of 150 m/min.

The effect of cutting speed on the white layer thickness is shown in Fig. 14. At the constant feed of 0.17 mm, the white layer thickness increases from 0 to 1.4 μm when the cutting speed increases from 100 to 160 m/min. This is due to the higher temperature produced at the higher cutting speed. However, as the cutting speed increases further to 200 m/min, the white layer thickness decreases to 0.8 μm. Although the temperature increases with increasing cutting speed, the shorter contact time between the tool and workpiece results in a shallower heat affected zone.

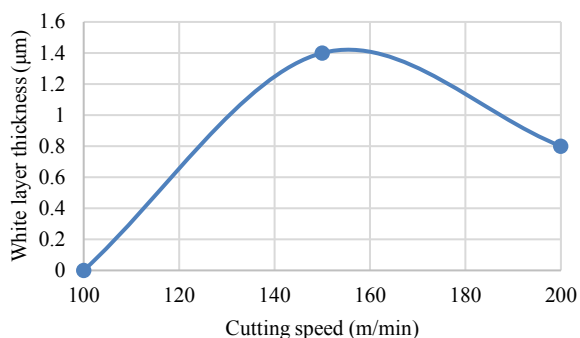


Fig. 14. White layer thickness at various cutting speeds and constant feed of 0.17 mm.

5. Conclusions

The 3D model was validated against the experimental results in terms of cutting forces. This 3D model was then simplified into 2D to reduce the simulation time. The 2D model was shown to be able to produce similar temperature results as the 3D model, and therefore, can be used to simulate thermally-induced phase transformation in a 3D turning process. The white layer results obtained from 2D simulation agree well with the experimental results with acceptable error below 12%. However, the 2D model could not predict the dark layer accurately. The simplification of the 3D turning process into 2D model significantly reduces the simulation time from 3-4 days to less than 24 hours based on a computer with Intel i7-5820L CPU@3.3GHz, 6 cores and 48GB RAM, while still ensuring high accuracy for white layer prediction.

The relationship between the white layer thickness with the cutting speed and the feed was also studied. With increasing feed, the white layer thickness increases. With increasing cutting speed, the white layer thickness first increases and reaches a maximum value. A further increase in cutting speed leads to a decrease in white layer thickness.

Acknowledgements

The authors acknowledge the Natural Sciences and Engineering Research Council of Canada (NSERC), and the Aerospace Manufacturing Technology Centre, National Research Council Canada (AMTC-NRC) for their financial support.

References

[1] A. Ramesh, S. N. Melkote, L. F. Allard, L. Riester, and T. R. Watkins, "Analysis of white layers formed in hard turning of AISI 52100 steel,"

- Materials Science and Engineering: A*, vol. 390, no. 1, pp. 88-97, 2005/01/15/ 2005, doi: <https://doi.org/10.1016/j.msea.2004.08.052>.
- [2] P. Arrazola and T. Özel, "Numerical modelling of 3-D hard turning using Arbitrary Eulerian Lagrangian finite element method," *Int. J. Machining and Machinability of Materials*, vol. 3, 01/01 2008, doi: 10.1504/IJMMM.2008.020907.
- [3] A. Attanasio, E. Ceretti, and C. Giardini, "3D FE MODELLING OF SUPERFICIAL RESIDUAL STRESSES IN TURNING OPERATIONS," *Machining Science and Technology*, vol. 13, no. 3, pp. 317-337, 2009/08/31 2009, doi: 10.1080/10910340903237806.
- [4] Y. B. Guo and C. Liu, "3D FEA modeling of hard turning," *Journal of Manufacturing Science and Engineering-transactions of The Asme - J MANUF SCI ENG*, vol. 124, 05/01 2002, doi: 10.1115/1.1430678.
- [5] O. Iynen, A. K. Ekşi, H. K. Akyıldız, and M. B. Özdemir, "Real 3D turning simulation of materials with cylindrical shapes using ABAQUS/Explicit," *Journal of the Brazilian Society of Mechanical Sciences and Engineering*, 2021.
- [6] R. Li and A. Shih, "Finite Element Modeling of 3D Turning of Titanium," *The International Journal of Advanced Manufacturing Technology*, vol. 29, 09/11 2006, doi: 10.1007/s00170-005-2511-6.
- [7] G. Liu, C. Huang, R. Su, T. Özel, Y. Liu, and L. Xu, "3D FEM simulation of the turning process of stainless steel 17-4PH with differently texturized cutting tools," *International Journal of Mechanical Sciences*, vol. 155, pp. 417-429, 2019/05/01/ 2019, doi: <https://doi.org/10.1016/j.ijmecsci.2019.03.016>.
- [8] M. Lotfi, M. Jahanbakhsh, and A. Akhavan Farid, "Wear estimation of ceramic and coated carbide tools in turning of Inconel 625: 3D FE analysis," *Tribology International*, vol. 99, pp. 107-116, 2016/07/01/ 2016, doi: <https://doi.org/10.1016/j.triboint.2016.03.008>.
- [9] T. Özel, "Computational modelling of 3D turning: Influence of edge micro-geometry on forces, stresses, friction and tool wear in PcBN tooling," *Journal of Materials Processing Technology*, vol. 209, no. 11, pp. 5167-5177, 2009/06/21/ 2009, doi: <https://doi.org/10.1016/j.jmatprotec.2009.03.002>.
- [10] *DEFORM Integrated 2D-3D v11.3 User's Manual*. (2022). Scientific Forming Technologies Corporation (SFTC), Columbus, Ohio.
- [11] H. Shin and J.-b. Kim, "A Phenomenological Constitutive Equation to Describe Various Flow Stress Behaviors of Materials in Wide Strain Rate and Temperature Regimes," *Journal of Engineering Materials and Technology*, vol. 132, 04/01 2010, doi: 10.1115/1.4000225.
- [12] B. Shi, H. Attia, and N. Tounsi, "Identification of Material Constitutive Laws for Machining—Part I: An Analytical Model Describing the Stress, Strain, Strain Rate, and Temperature Fields in the Primary Shear Zone in Orthogonal Metal Cutting," *Journal of Manufacturing Science and Engineering*, vol. 132, p. 051008, 10/01 2010, doi: 10.1115/1.4002454.
- [13] B. Shi, H. Attia, and N. Tounsi, "Identification of Material Constitutive Laws for Machining—Part II: Generation of the Constitutive Data and Validation of the Constitutive Law," *Journal of Manufacturing Science and Engineering*, vol. 132, p. 051009, 10/01 2010, doi: 10.1115/1.4002455.
- [14] S. A. Iqbal, P. T. Mativenga, and M. A. Sheikh, "An investigative study of the interface heat transfer coefficient for finite element modelling of high-speed machining," *Proceedings of the Institution of Mechanical Engineers, Part B: Journal of Engineering Manufacture*, vol. 222, no. 11, pp. 1405-1416, 2008/11/01 2008, doi: 10.1243/09544054JEM1179.
- [15] D. Umbrello, A. D. Jayal, S. Caruso, O. W. Dillon, and I. S. Jawahir, "Modeling of white and dark layer formation in hard machining of AISI 52100 bearing steel," *Machining Science and Technology*, vol. 14, no. 1, pp. 128-147, 2010/02/26 2010, doi: 10.1080/10910340903586525.
- [16] F. Zhang, C. Duan, W. Sun, and K. Ju, "Effects of cutting conditions on the microstructure and residual stress of white and dark layers in cutting hardened steel," *Journal of Materials Processing Technology*, vol. 266, pp. 599-611, 2019/04/01/ 2019, doi: <https://doi.org/10.1016/j.jmatprotec.2018.11.038>.